Theory of dynamic arrest in colloidal mixtures

R. Juárez-Maldonado and M. Medina-Noyola
Instituto de Física "Manuel Sandoval Vallarta," Universidad Autónoma de San Luis Potosí, Álvaro Obregón 64, 78000 San Luis Potosí, SLP, México

(Received 10 November 2007; revised manuscript received 18 February 2008; published 23 May 2008)

We present a first-principles theory of dynamic arrest in colloidal mixtures based on the multicomponent self-consistent generalized Langevin equation theory of colloid dynamics [M. A. Chávez-Rojo and M. Medina-Noyola, Phys. Rev. E **72**, 031107 (2005); **76**, 039902 (2007)]. We illustrate its application with a description of dynamic arrest in two simple model colloidal mixtures: namely, hard-sphere and repulsive Yukawa binary mixtures. Our results include observation of the two patterns of dynamic arrest, one in which both species become simultaneously arrested and the other involving the sequential arrest of the two species. The latter case gives rise to mixed states in which one species is arrested while the other species remains mobile. We also derive the ("bifurcation" or fixed-point") equations for the nonergodic parameters of the system, which takes the surprisingly simple form of a system of coupled equations for the localization length of the particles of each species. The solution of this system of equations indicates unambiguously which species is arrested (finite localization length) and which species remains ergodic (infinite localization length). As a result, we are able to draw the entire ergodic-nonergodic phase diagram of the binary hard-sphere mixture.

DOI: 10.1103/PhysRevE.77.051503 PACS number(s): 64.70.Q−

I. INTRODUCTION

The fundamental understanding of dynamically arrested states is a major challenge of contemporary statistical physics and materials science [1–3]. Model experimental colloidal suspensions, whose dynamics has been the subject of study on its own right [4–6], have played an essential role in the study of dynamic arrest phenomena, providing experimental realizations in finely controlled systems and conditions [7–11]. Thus, it is an experimental fact that by changing a macroscopic control parameter such as the volume fraction or by tuning the effective interparticle interactions, one may drive the system from the region of equilibrium (ergodic) states to the region of dynamically arrested (nonergodic) states. First-principles models and theories that predict and describe these transitions thus constitute an essential aspect of the fundamental understanding of these phenomena. The mode-coupling theory (MCT) of the ideal glass transition [3,12] is perhaps the most comprehensive theory of this sort, some of whose predictions have found beautiful experimental confirmation [7,10,11]. Many issues, however, still remain to be understood, and this has prompted the proposal of extended versions of this theory [13–15] or the development of alternative approaches [16].

In this context, in recent work a first-principles theory of dynamic arrest has been proposed [17–19] which is essentially the application of the self-consistent generalized Langevin equation (SCGLE) theory of colloid dynamics [20–23] to the analysis of dynamic arrest phenomena in colloidal systems. The SCGLE theory was originally devised to describe the tracer and collective diffusion properties of colloidal dispersions in the short- and intermediate-times regimes. Its self-consistent character, however, introduces a nonlinear dynamic feedback, leading to the prediction of dynamic arrest in these systems, similar to that exhibited by the mode-coupling theory of the ideal glass transition. The resulting theory of dynamic arrest in colloidal dispersions was applied in recent work to describe the glass transition in three monodisperse experimental systems with specific (hard-sphere, screened electrostatic, and depletion) interparticle effective forces [17,18], with the same quantitative predictive power as conventional MCT, but with a smaller degree of difficulty in its application [19]. The present paper introduces the multicomponent extension of the SCGLE theory of colloid dynamics [24,25] as an alternative first-principles theory of dynamic arrest in colloidal mixtures.

Colloidal mixtures offer a richer variety of possible dynamic arrest scenarios [26–31]. These include, for example, the possibility that the particles of one species become arrested, while the particles of the other species continue to diffuse through the disordered matrix of the arrested particles. In fact, an important prediction of the multicomponent extension of MCT [32,33] was precisely the existence of these mixed states [34–36]. Later studies of dynamic arrest in mixtures [37–42] have been based on MCT not because it is the ultimate and definitive theory, but because it was virtually the only first-principles theory of dynamic arrest available that had a high level of predictive capability. However, relevant issues remain that have not been resolved by its application. For example, although the one-component version of MCT predicts the existence of repulsive glasses in a hard-sphere system and its melting upon the addition of a small amount of smaller particles (depletion forces), followed by the reentrance to a new kind of (attractive) glass [10], no reentrance seems to be predicted by the two-component version of MCT [43]. Issues like this merit the development of alternative approaches to the description of dynamic arrest phenomena in mixtures, particularly if they are independent from conventional MCT. Although the SCGLE theory presented here has several features in common with MCT, such as its use of exact memory function expressions for the concentration-concentration time-correlation functions, in the SCGLE theory the derivations, approximations, and argumentation are conceived and based

on a totally different fundamental and conceptual framework [20–25].

Besides presenting the SCGLE theory of dynamic arrest in colloid mixtures, in the present paper we illustrate the scenarios predicted by this theory in the simplest conditions: namely, in its application to model binary mixtures. For two such systems, a repulsive Yukawa mixture and a hard-sphere mixture, we numerically solve the full self consistent system of dynamic equations for the so-called propagators (or Green's functions) of the self- and collective intermediate scattering functions. We illustrate in this manner the two possible dynamic arrest patterns possible in a binary colloidal mixture: namely, the simultaneous and the sequential arrest of the two species. In the latter case, we discuss the hybrid or partially arrested states in which one species is dynamically arrested while the other species remains ergodic.

Determining the location of the ergodic-nonergodic transitions and calculating the nonergodic parameters may be done by solving the self-consistent system of equation or, more simply, by finding the long-time asymptotic stationary ("fixed-point") solutions of the self-consistent system of equations. Here we also address this issue and report the derivation of a strikingly simple and general result which takes the form of a system of coupled equations for the localization length of the particles of each species. Solving this system of equations leads to the unambiguous identification of which species is arrested (finite localization length) and which species remains ergodic (infinite localization length). As a result, we are able to draw the entire ergodic-nonergodic phase diagram of the binary hard-sphere mixture, which is one of the main specific contributions of this work.

The present paper starts with a brief summary of the SCGLE theory of the dynamics of colloidal mixtures. This theory was developed in Ref. [25] and tested there through its comparison with the short- and intermediate-time results of Brownian dynamics computer simulations for a model colloidal mixture interacting through screened Coulomb pair interactions. That original version of the SCGLE theory required as an input not only the partial static structure factors, but also other equilibrium static structural information associated with the exact short-time conditions that this initial version of the theory aimed at incorporating. As has been shown more recently [19], however, a simplified version of the SCGLE theory, in which this exact short-time information is neglected, happens to be equally accurate, particularly in the long-time regime and with respect to the predicted dynamic arrest scenarios. Thus, we shall refer to this simplified version simply as the SCGLE theory, which we review in the following section.

Although our main interest here is in the description of dynamic arrest phenomena, in Sec. III we start our discussion by reviewing the predictive capability of this simplified theory in the short- and intermediate-time regimes of the model binary Yukawa mixture studied in Ref. [25] in one of the fully ergodic states considered in that work. We then proceed to illustrate the dynamic arrest scenarios predicted by this theory by taking as the initial reference the same repulsive Yukawa mixture and increasing the intensity of the repulsion parameter (a process that amounts to effectively lowering the temperature) until reaching a transition to a dynamically arrested state. This turns out to be a transition from a fully ergodic to a fully arrested state in which both species are simultaneously arrested. In the second of our illustrative examples, in Sec. IV we consider a hard-sphere model colloidal mixture, whose state parameters are the size disparity and the concentration of the two species. Here we present an example of a transition to a partially arrested state, in which the large particles become arrested and the smaller particles continue to diffuse in the disordered matrix formed by the arrested species. In Sec. V we derive the equations for the nonergodic parameters of the system and illustrate its use in the context of the hard-sphere binary mixture by determining its entire dynamic-arrest phase diagram. The main conclusions of this paper are finally summarized in Sec. VI.

II. SCGLE THEORY OF THE DYNAMICS OF COLLOIDAL MIXTURES

In this section we summarize the main elements of the self-consistent theory of the dynamics of colloidal mixtures presented in Refs. [24,25]. For a colloidal mixture with ν species, the dynamic properties can be described in terms of the relaxation of the fluctuations $\delta n_\alpha(\mathbf{r},t)$ of the local concentration $n_\alpha(\mathbf{r},t)$ of colloidal particles of species α $(=1,2,\ldots,\nu)$ around its bulk equilibrium value n_α. The average decay of $\delta n_\alpha(\mathbf{r},t)$ is described by the time-dependent correlation function $F_{\alpha\beta}(k,t)\equiv\langle \delta n_\alpha(\mathbf{k},t)\delta n_\beta(-\mathbf{k},0)\rangle$ of the Fourier transform $\delta n_\alpha(\mathbf{k},t)\equiv(1/\sqrt{N_\alpha})\Sigma_{i=1}^{N}\exp[i\mathbf{k}\cdot\mathbf{r}_i^{(\alpha)}(t)]$ of the fluctuations $\delta n_\alpha(\mathbf{r},t)$, with $\mathbf{r}_i^{(\alpha)}(t)$ being the position of particle i of species α at time t. $F_{\alpha\beta}(k,t)$ is referred to as the partial intermediate scattering function, measured by experimental techniques such as dynamic light scattering [4,6]. One can also define the *self*-component of $F_{\alpha\beta}(k,t)$, referred to as the self-intermediate scattering function, as $F_{\alpha\beta}^{(s)}(k,t)\equiv\delta_{\alpha\beta}\langle\exp[i\mathbf{k}\cdot\Delta\mathbf{R}^{(\alpha)}(t)]\rangle$, where $\Delta\mathbf{R}^{(\alpha)}(t)$ is the displacement of any of the N_α particles of species α over a time t and $\delta_{\alpha\beta}$ is Kronecker's delta function.

For notational economy, let us denote the *matrix* with elements $F_{\alpha\beta}(k,t)$ $(\alpha,\beta=1,2,\ldots,\nu)$ by $F(k,t)$ or simply by $F(t)$, and similarly for $F^{(s)}(t)$. These matrices have the initial values $F(t=0)=S$ and $F^{(s)}(t=0)=I$, where I is the identity matrix $I_{\alpha\beta}\equiv\delta_{\alpha\beta}$ and the elements of the matrix S are the partial static structure factors $S_{\alpha\beta}(k)\equiv\langle\delta n_\alpha(\mathbf{k},0)\delta n_\beta(-\mathbf{k},0)\rangle$. The matrix of intermediate scattering functions may also be normalized by its initial value to define the *collective propagator* matrix $\Psi(t)\equiv F(t)S^{-1}$, which is such that $\Psi(0)=I$. In a similar manner, we define the *self-propagator* matrix as $\Psi^{(s)}(t)\equiv F^{(s)}(t)$, normalized to $\Psi^{(s)}(0)=I$.

The multicomponent version of the SCGLE theory starts with the exact time-evolution equation that governs the relaxation of the Fourier transform $\delta n_\alpha(\mathbf{k},t)$ of the fluctuations of the local concentration of species α. This equation also governs the relaxation of the partial intermediate scattering functions $F_{\alpha\beta}(k,t)$ and can be written as an exact expression for the Laplace transform (LT) $F(z)$ of the matrix $F(t)$: namely [24],

$$F(z)=\{z+[I+C(z)]^{-1}k^2DS^{-1}\}^{-1}S, \tag{2.1}$$

where the elements of the matrix D are given by $D_{\alpha\beta}\equiv\delta_{\alpha\beta}D_\alpha^0$, with D_α^0 being the diffusion coefficient of species α

in the absence of interactions. This is related to the solvent friction coefficient on an isolated particle of species α, ζ_α^0, through the Einstein relation $D_\alpha^0 \equiv k_B T/\zeta_\alpha^0$. The elements $C_{\alpha\beta}(k,z)$ of the matrix $C(z)$ are the LT of the so-called irreducible memory functions $C_{\alpha\beta}(k,t)$ [36,44]. The corresponding result for the "self"-component, $F^{(s)}(z)$ of the matrix $F(z)$ reads

$$F^{(s)}(z) = \{z + [I + C^{(s)}(z)]^{-1} k^2 D\}^{-1}, \tag{2.2}$$

where the matrix $C^{(s)}(z)$ is the corresponding irreducible memory function.

The second ingredient of the SCGLE theory is the intuitive notion that collective and self-dynamics may be connected in a simple manner. Vineyard's approximation [45], in which $F(t)S^{-1} = \Psi(t)$ is approximated by $F^{(s)}(t) = \Psi^{(s)}(t)$, is the most primitive (or "zeroth-order") implementation of this idea. Equations (2.1) and (2.2) suggest, however, that other connections between self-dynamics and collective dynamics may be proposed at the level of the memory functions $C(k,z)$ and $C^{(s)}(k,z)$, the simplest of them being to approximate one by the other: namely,

$$C(t) = C^{(s)}(t). \tag{2.3}$$

This will be referred to as the first-order Vineyard approximation and is the approximation that we shall incorporate in the SCGLE theory of dynamic arrest introduced in the present work. In spite of its apparent simplicity (or, in fact, because of its simplicity), this turns out to be the formal connection between collective and self-dynamics that best serves the purpose of describing the long-time slow dynamics of systems near their dynamic arrest transitions. It is the best not only because it is the simplest, but also because it turns out to be equally accurate, for the purpose above, as other more sophisticated higher-order Vineyard approximations. For the sake of clarity, let us explain further this appreciation.

The accuracy and usefulness of the Vineyard approximation above depends, of course, on the specific purpose of its use. Thus, imagine that one calculates exactly (e.g., by computer simulations) both $F(k,t)$ and $F^{(s)}(k,t)$ for a system far from its dynamic arrest transition and that from these properties, using Eqs. (2.1) and (2.2), one extracts the exact memory functions $C(k,t)$ and $C^{(s)}(k,t)$. Direct comparison of these functions will then exhibit natural and expected differences, as illustrated, for example, by Cichocki and Hinzen [46] in moderately concentrated hard-sphere suspensions for relatively short relaxation times. Under such conditions, it may not be advisable to resort to the simple approximation above and one might have to consider higher-order Vineyard approximations which do incorporate the correct short-time behavior. This issue was discussed by Yeomans-Reyna *et al.* [21], who proposed and tested an array of higher-order Vineyard approximations. In fact, the original proposal of the SCGLE theory [22–24], aimed at describing the dynamics of systems in the short- and intermediate-time regimes far from dynamic arrest conditions, did not involve the first-order Vineyard approximation above. Instead, it considered the incorporation of either of two higher-order connections, referred to as the additive and multiplicative Vineyard-like approximations. The first approximates the difference $[C(k,z) - C^{(s)}(k,z)]$ and the second the ratio $[C(k,z)C^{(s)-1}(k,z)]$ of the memory functions by their exact short-time limits using the fact that the exact short-time expressions $C^{\text{sexp}}(k,t)$ and $C^{(s),\text{sexp}}(k,t)$ of these memory functions are known in terms of equilibrium structural properties [47]. The multiplicative approximation was devised to describe more accurately the very early relaxation of $F(k,t)$ [23], but the additive approximation was eventually found to be equally accurate and definitely simpler to apply to colloidal mixtures [24]. Furthermore, it was also found to provide a simpler and more accurate description of the glass transition in monodisperse systems [18]. More recently, however, it was also realized [19] that in the vicinity of the glass transition, the asymptotic long-time solutions of the resulting SCGLE theory coincide with those of a still simpler version of the SCGLE theory in which the additive approximation $[C(k,z) - C^{(s)}(k,z)] = [C^{\text{sexp}}(k,t) - C^{(s),\text{sexp}}(k,t)]$ is replaced by the first-order Vineyard approximation in Eq. (2.3). The reason for this is that the information involved in the short-time functions $C^{\text{sexp}}(k,t)$ and $C^{(s),\text{sexp}}(k,t)$ is only relevant at very short times and these functions decay very fast compared with the relevant time scales associated with the slow relaxation times near the glass transition. Thus, regarding the description of dynamic arrest, the SCGLE theory complemented with the first-order Vineyard approximation above is just as accurate as the SCGLE theory complemented with the additive Vineyard approximation, but it is much simpler because it does not require knowledge of the short-time properties $C^{\text{sexp}}(k,t)$ and $C^{(s),\text{sexp}}(k,t)$. A most notorious feature, however, is the fact that the accuracy of the resulting self-consistent scheme is not restricted to the strictly long-time regime, but also applies to the short- and intermediate-time regimes to a rather unexpected extent [19]. Independently of that, in this work we adopt the first-order Vineyard approximation in Eq. (2.3) as the second element of the present SCGLE theory because this work deals only with the description of dynamic arrest transitions.

The third ingredient of the SCGLE theory was suggested [25] as the interpolation of $C^{(s)}(t)$ between its two exact limits at small and large wave vectors by means of a phenomenological but universal interpolation device. We know that the $C^{(s),\text{sexp}}(t)$ is also the exact large-k limit of $C^{(s)}(t)$, whereas the small-k limit is the so-called time-dependent friction function matrix $\Delta\zeta^*(t)$ [5,22,25]. Thus, we write $C^{(s)}(k,t) = C^{(s),\text{sexp}}(k,t) + [\Delta\zeta^*(t) - C^{(s),\text{sexp}}(k,t)]\lambda(k)$, where we have written explicitly the k dependence of the various matrices. The matrix λ is a matrix of phenomenological interpolating functions, whose elements are defined as [22,25]

$$\lambda_{\alpha\beta}(k) \equiv \delta_{\alpha\beta}/[1 + (k/k_{\text{min}}^{(\alpha)})^2], \tag{2.4}$$

with $k_{\text{min}}^{(\alpha)}$ being the position of the first minimum following immediately the main peak of the partial static structure factor $S_{\alpha\alpha}(k)$. At times long enough that the short-time memory function $C^{(s),\text{sexp}}(k,t)$ has already decayed, the interpolation formula above for $C^s(k,t)$ simplifies still further, reading

$$C^{(s)}(k,t) = [\Delta\zeta^*(t)]\lambda(k). \tag{2.5}$$

As suggested in Ref. [19], it is this approximation that enters in the present formulation of the multicomponent SCGLE theory of dynamic arrest.

The matrix $\Delta\zeta^*(t)$ in Eq. (2.5) is a diagonal matrix whose αth diagonal element $\Delta\zeta^*_\alpha(t)$ is the time-dependent friction function of particles of species α. The final ingredient of the SCGLE theory is an approximate but general result for this property, which, as explained below, was derived as an application of the GLE formalism [48–50] to tracer diffusion phenomena. Such an expression reads [50]

$$\Delta\zeta^*_\alpha(t) = \frac{D^0_\alpha}{3(2\pi)^3}\int d^3k\, k^2[F^{(s)}(t)]_{\alpha\alpha}[c\sqrt{n}F(t)S^{-1}\sqrt{n}h]_{\alpha\alpha}, \tag{2.6}$$

with the elements of the k-dependent matrices h and c being the Fourier transforms $h_{\alpha\beta}(k)$ and $c_{\alpha\beta}(k)$ of the Ornstein-Zernike total and direct correlation functions, respectively. Thus, h and c are related to S by $S=I+\sqrt{n}h\sqrt{n}=[I-\sqrt{n}c\sqrt{n}]^{-1}$, with the matrix $\sqrt{n}$ defined as $[\sqrt{n}]_{\alpha\beta}\equiv\delta_{\alpha\beta}\sqrt{n_\alpha}$.

Let us now comment on the origin of Eq. (2.6). In Ref. [48] the effective Langevin equation of a tracer colloidal particle interacting with the other particles of a monodisperse suspension was derived using the concept of contraction of the description [49] (a summary of such derivation is contained in Appendix B of Ref. [18]). Besides the solvent friction force $-\zeta^0\mathbf{V}(t)$, the direct interactions of the tracer particle with the other particles give rise to an additional friction term of the form $-\int_0^t dt'\,\Delta\zeta(t-t')\mathbf{V}(t')$, where $\mathbf{V}(t)$ is the tracer particle's velocity at time t. In the process, an exact result for the time-dependent friction function $\Delta\zeta^*(t)\equiv\Delta\zeta(t)/\zeta^0$ is generated which, when complemented with two well-defined approximations, leads to the monodisperse version of Eq. (2.6). The multicomponent extension was derived in Ref. [50] from the exact result in Eq. (124) of that reference, upon the introduction of the "homogeneous fluid" and the "decoupling" approximations [Eqs. (135)–(138) and (144) of the same reference].

Finally, let us mention that Eqs. (2.1) and (2.2) are exact results and that Eq. (2.6) derives from the exact result just referred to. Hence, it should not be a surprise that the same results are employed by other theories; in fact, these equations also appear in the formulation of MCT. The difference lies, of course, in the way we relate them and use them; in this sense, the distinctive elements of our theory are then the Vineyard-like approximation in Eq. (2.3) and the factorization approximation in Eq. (2.5).

III. ILLUSTRATIVE APPLICATION: THE MODEL YUKAWA MIXTURE

The set of coupled equations (2.1)–(2.6) constitutes the self-consistent generalized Langevin equation theory of the dynamics of colloidal mixtures and has to be solved numerically. For this, Eqs. (2.1) and (2.2) are first Laplace inverted and written as a set of coupled integro-differential equations involving functions of k and t. These functions are then discretized in a mesh of points large enough to ensure independence of the solution with respect to the size of the mesh. The discretized system of equations is then solved by a straightforward direct iteration method or, for the long times required in the study of dynamic arrest phenomena, by the methods described in Refs. [51,52].

To illustrate its quantitative accuracy, the SCGLE theory was applied in Ref. [25] to the calculation of the dynamic properties of a particular model system: namely, a binary mixture of Brownian particles interacting through a hard-core pair potential of diameter σ, assumed the same for both species, plus a repulsive Yukawa tail of the form (in units of the thermal energy $k_BT=\beta^{-1}$)

$$\beta u_{\alpha\beta}(r) = A_\alpha A_\beta \frac{e^{-z(r/\sigma-1)}}{r/\sigma}. \tag{3.1}$$

The dimensionless parameters that define the thermodynamic state of this system are the total volume fraction $\phi\equiv\frac{\pi}{6}n\sigma^3$ (with n being the total number concentration, $n=n_1+n_2$), the relative concentrations $x_\alpha\equiv\frac{n_\alpha}{n}$ ($\alpha=1,2$), and the potential parameters A_1, A_2, and z. As in Ref. [25], here we also assume that the free-diffusion coefficients D^0_α of both species are identical—i.e., $D^0_1=D^0_2=D^0$. Explicit values of the parameters σ and D^0 are not needed, since the dimensionless dynamic properties, such as $F_{\alpha\beta}(k,t)$, only depend on the dimensionless parameters specified above, when expressed in terms of the scaled variables $k\sigma$ and t/t_0, where $t_0\equiv\sigma^2/D^0$. In Ref. [25] Brownian dynamics simulations were reported for the static and dynamic properties of this system with fixed screening parameter $z=0.15$ and various coupling parameters A_1 and A_2 and volume fractions in the short- and intermediate-time regimes.

The partial static structure factors $S_{\alpha\beta}(k)$ obtained from those simulations are also employed here as the static input needed in the implementation of the SCGLE theory. As a result, we can calculate all the dynamic properties entering in the self-consistent equations above and other properties that derive from them, such as the mean-squared displacements $W_\alpha(t)\equiv\langle[\Delta\mathbf{R}^{(\alpha)}(t)]^2\rangle/6$ or the time-dependent diffusion coefficients $D_\alpha(t)\equiv W_\alpha(t)/t$. In Fig. 1 a comparison of these results with the Brownian dynamics calculations is presented, involving the case of a binary mixture with $z=0.15$, $A_1=10$, and $A_2=10\sqrt{5}$. The volume fraction of the more interacting species is kept fixed at $\phi_2=2.2\times10^{-4}$, and ϕ_1 takes the values $\phi_1=0.725\times10^{-4}$ (left column), $\phi_1=2.2\times10^{-4}$ (middle column), and $\phi_1=6.6\times10^{-4}$ (right column), corresponding to molar fractions $x_1=0.25$, $x_1=0.5$, and $x_1=0.75$, respectively. This figure corresponds to the same conditions as Fig. 3 of Ref. [25] and illustrates the fact that the present *simplified* SCGLE theory also provides an excellent description of the relaxation of concentration fluctuations in colloidal suspensions in the short- and intermediate-time regimes illustrated in the figure. We notice that the largest departures of the theoretical results from the simulation data appear only at the short times illustrated by the time $t=t_0$, but the agreement improves at longer times, as illustrated by the time $t=10t_0$. The main message of this figure is that the present self-consistent theory of colloid dynamics provides

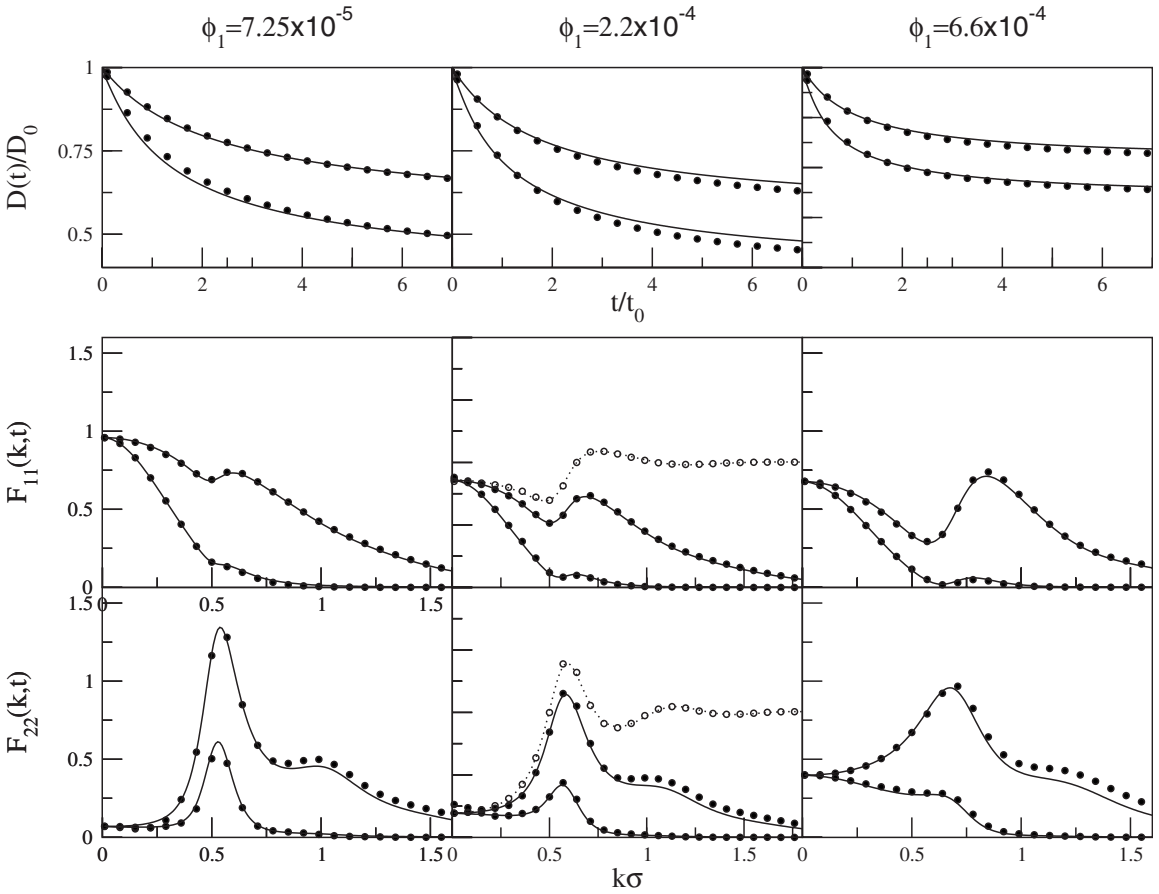

FIG. 1. Time-dependent diffusion coefficients $D_\alpha(t)$ as a function of time [upper curves corresponding to $D_1(t)$] and partial intermediate scattering functions $F_{11}(k,t)$ and $F_{22}(k,t)$ as a function of the wave vector of a repulsive Yukawa mixture with $z=0.15$, $A_1=10$, and $A_2=10\sqrt{5}$ for $t=t_0$ and $t=10t_0$. The volume fraction of the more interacting species is kept fixed at $\phi_2=2.2\times10^{-4}$, and ϕ_1 takes the values $\phi_1=0.725\times10^{-4}$ (left column), $\phi_1=2.2\times10^{-4}$ (middle column), and $\phi_1=6.6\times10^{-4}$ (right column). Solid lines are the SCGLE theoretical results, and circles are Brownian dynamics data. In the middle column we also include the partial static structure factors $S_{\alpha\alpha}(k)\equiv F_{\alpha\alpha}(k,t=0)$, with the dotted lines being a smooth HNC-fit of the simulation data.

an adequate description of the dynamic properties of a simple idealized mixture also in the short- and intermediate-time regimes, even though it does not satisfy the exact short-time conditions built in the original proposal of this theory [25]. With this confidence, let us now explore the long-time regime under conditions typical of the vicinity of a transition to dynamically arrested states.

For this, let us take the conditions of the middle column of Fig. 1 as a reference and let us keep the parameters ϕ_1, ϕ_2, and z fixed ($\phi_1=\phi_2=2.2\times10^{-4}$ and $z=0.15$) while we increase the coupling parameters A_1 and A_2 in an identical proportion to mimic a process of lowering the temperature. Thus, let us write $A_\alpha=A_\alpha^0\chi$ ($\alpha=1,2$), with $A_1^0=10$ and $A_2^0=10\sqrt{5}$, and increase χ from its unit value in Fig. 1 until a transition of dynamic arrest is encountered. In this case, we do not run computer simulations to provide the input partial static structure factors needed in the self-consistent scheme. Instead, we resort to an approximate liquid-state theory: namely, the solution of the Ornstein-Zernike integral equation within the hypernetted-chain (HNC) approximation [53]. In doing this we only lose quantitative precision, but not qualitative accuracy. In fact, the HNC approximation will yield the same scenario, but at effective values of the coupling parameters A_1 and A_2 larger than the actual ones. For example, the fitting curves for the partial static structure factors in the middle column of Fig. 1 were obtained using the HNC approximation with effective coupling parameters given by $A_\alpha=A_\alpha^0\chi$ with $\chi=1.225$.

In Fig. 2 we present the results of the SCGLE theory for the diagonal elements $\Psi_{\alpha\alpha}(k,t)$ of the collective propagator matrix $\Psi(t)$ as a function of time for fixed wave vector $k=k_{\max}$, where $k_{\max}$ is the position of the main peak of the corresponding static structure factor $S_{\alpha\alpha}(k)$. This figure illustrates the fact that as we lower the temperature starting from the reference state ($\chi=1.225$) the system reaches eventually a transition to an arrested state. This occurs for $A_1=42.57$ and $A_2=95.19$—i.e., for $\chi=4.257$—and this is a transition from a fully ergodic to a fully arrested state; i.e., both species become simultaneously arrested. This is evidenced by the fact that below this threshold condition, exemplified in the figure by the case $\chi=4.255$, both propagators decay to zero, whereas above this condition, exemplified by the case $\chi=4.330$, they decay to a finite nonergodic value. Thus, the nonergodic parameters jump discontinuously at the transition from zero in the ergodic side to finite values in the glass side. Exactly the same behavior is exhibited by the self-diffusion

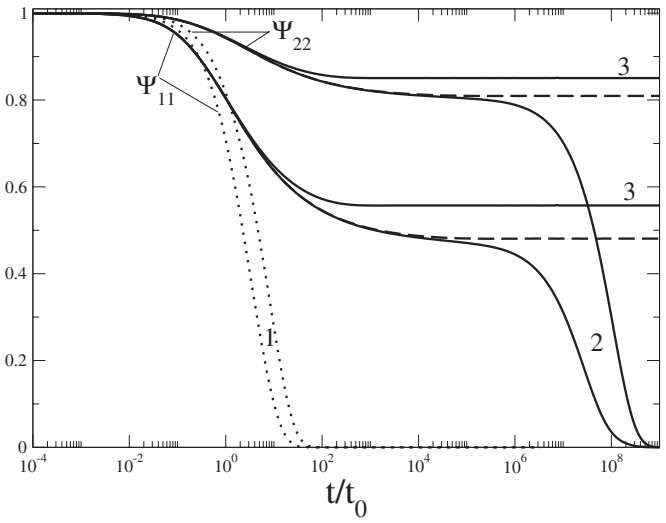

FIG. 2. SCGLE results for the collective diffusion propagators $\Psi_{\alpha\alpha}(k_{\max},t)$ at fixed wave vector $k_{\max}$ [the position of the main peak of $S_{\alpha\alpha}(k)$] for the Yukawa mixture with $z=0.15$, $\phi_1=\phi_2=2.2\times10^{-4}$ calculated using HNC partial static structure factors evaluated at effective coupling parameters given by $A_\alpha=A_\alpha^0\chi$, with $A_1^0=10$ and $A_2^0=10\sqrt{5}$, for values of χ corresponding to the reference state in Fig. 1 ($\chi^{(1)}=1.225$, curves labeled "1") and to states slightly below ($\chi^{(2)}=4.255$, labeled "2") and above ($\chi^{(3)}=4.330$, labeled "3") the dynamic arrest transition. The dashed plateaus indicate the value of the nonergodicity parameters right at the transition ($\chi=4.257$).

propagators $\Psi_{11}^{(s)}(k,t)$ and $\Psi_{22}^{(s)}(k,t)$, not included in the present illustration. Let us stress that this process of increasing A_1 and A_2 keeping z fixed is a mathematical, rather than physical, exercise; the practicable experimental manner to increase A_1 and A_2 would be to increase the particle's electric charge (or to lower the dielectric constant of the solvent), which in reality would also increase the screening parameter z. Here, however, we use this exercise only to illustrate the pattern of dynamic arrest transition in colloidal mixtures in which the particles of both species become localized simultaneously.

Similar calculations can be carried out for other regions of the parameter space $(\phi_1,\phi_2,A_1,A_2,z)$, but this scanning and its results in terms of other possible regions that exhibit interesting dynamic behavior constitute an independent issue beyond our current objective of introducing our SCGLE theory of dynamic arrest in mixtures and illustrating its use. We can mention, however, that in other regions of this state space the theory predicts also the other pattern of dynamic arrest, which we now illustrate in the context of a simpler system: namely, the hard-sphere colloidal mixture.

IV. HARD-SPHERE MIXTURE

Let us now consider the binary hard-sphere model dispersion—i.e., the uncharged version of the previous system in which we now allow for hard-sphere size disparity. Thus, we consider two species of particles of hard-core diameters σ_1 and σ_2, present at concentrations n_1 and n_2. We use as dimensionless control parameters the size asymmetry $\delta\equiv\sigma_1/\sigma_2\leq1$ and either the two volume fractions ϕ_1 and ϕ_2 (with $\phi_\alpha\equiv\pi n_\alpha\sigma_\alpha^3/6$) or the total packing fraction $\phi=\phi_1+\phi_2$ together with the molar fraction of the smaller species, $x_1=n_1/(n_1+n_2)$. This system serves to illustrate some features associated precisely with the size disparity. As discussed in more detail below, one expects that for mild asymmetries the only possible mode of dynamic arrest for all volume fractions and all molar fractions is that in which both species are arrested simultaneously. It is only in the regime of disparate sizes that one expects a richer scenario, including the second mode of dynamic arrest, in which the large particles are first arrested while the other species continues to diffuse, followed by a second transition at a higher total volume fraction in which the smaller particles are finally localized inside the pores of the matrix formed by the previously arrested particles. Thus, there must be a threshold asymmetry δ_c beyond which this might occur. One also expects, however, that even in the regime of considerable size disparities, but for conditions corresponding to a few large particles in a sea of smaller ones, the only mode of dynamic arrest continues to be the mode of simultaneous dynamic arrest of the two species, since in this case the arrest of the small particles implies the arrest of the few large ones. We call this the "chancaquilla" limit [54], in reference to one of the many names of a rather universal sweet prepared by the vitrification of liquid molasses in which nuts or raisins are previously dispersed. Clearly, the dynamic arrest of the supporting molasses implies the arrest of the nuts dispersed in it. Hence, for large-size asymmetries we expect to find both modes of dynamic arrest located in the neighborhood of the opposite composition limits $x_1=0$ and $x_1=1$.

In fact, this is exactly the scenario predicted by our theory. We illustrate this with the SCGLE results obtained using the Percus-Yevick [55] structure factors as the static input for a size asymmetry $\delta=0.3$. Let us calculate the collective and self-propagator matrices $\Psi(t)$ and $\Psi^{(s)}(t)$ at increasing total volume fractions ϕ starting in the ergodic regime, crossing the dynamic arrest transition line, and ending inside the regime of arrested states. If this is done in the neighborhood of the $x_1=1$ axis, say, for $x_1=0.8$, the scenario would be essentially that described by the chancaquilla mechanism involving the simultaneous dynamic arrest of both species with similar results to those discussed in Fig. 2 for the Yukawa mixture. The other mode of dynamic arrest is observed in the opposite regime, where the small particles are a minority, exemplified by the molar fraction $x_1=0.2$. This case is illustrated in Fig. 3, which presents the evolution of the relaxation of the diagonal elements of the collective and self-propagator matrices $\Psi(t)$ and $\Psi^{(s)}(t)$ as we increase the total volume fraction ϕ at fixed molar fraction $x_1=0.2$, starting in the ergodic regime. We find that, rather than passing directly from the fully ergodic region to the region of fully arrested states, as in Fig. 2, one first passes through an intermediate region of hybrid states, in which only the large particles are arrested, but the small particles continue to diffuse. Thus, at a volume fraction $\phi_g^{(1)}\approx0.545$, the system passes from the fully ergodic region to the region $\phi_g^{(1)}<\phi<\phi_g^{(2)}$ of hybrid states, with $\phi_g^{(2)}$ being the location of the second transition consisting of the localization of the small particles in the pores of the random matrix of large particles.

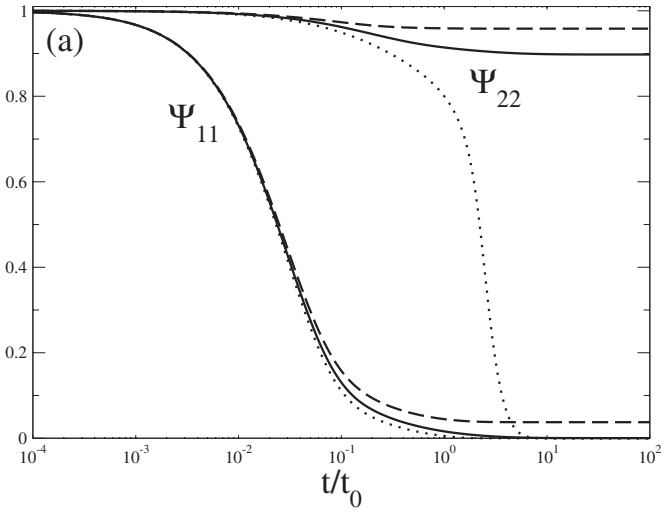

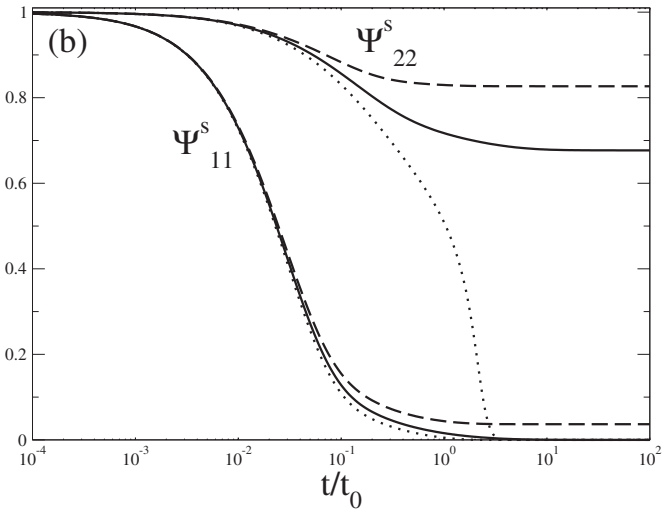

FIG. 3. (a) Collective diffusion propagators $\Psi_{\alpha\alpha}(k_{\max},t)$ and (b) self-diffusion propagators $\Psi^{(s)}_{\alpha\alpha}(k_{\max},t)$ at fixed wave vector $k_{\max}$ [the position of the main peak of $S_{\alpha\alpha}(k)$] for the hard-sphere mixture with $\delta=0.3$ and $x_1=0.2$ for different total packing fraction ϕ. The results for $\phi=0.53$ (dotted lines) illustrate the fully ergodic states, whereas those for $\phi=57$ (dashed lines) illustrate the fully arrested states, in which both species are arrested. The results for $\phi=0.55$ (solid lines) illustrate the hybrid states in which the large particles are arrested while the smaller particles continue to diffuse.

In the present example this occurs at $\phi_g^{(2)}\approx 0.555$.

Let us mention that in all these cases one observes that the diagonal collective diffusion propagator $\Psi_{\alpha\alpha}(k,t)$ behaves in qualitatively identical manner to the corresponding self-diffusion propagator $\Psi^{(s)}_{\alpha\alpha}(k,t)$ in the sense that either both relax to zero or both exhibit dynamic arrest (i.e., decay to a finite value). One does not encounter a situation in which, for example, $\Psi_{11}(k,t)$ decays to a finite value while $\Psi^{(s)}_{11}(k,t)$ decays to zero. This indicates that at the level of the diagonal propagators, self-diffusion and collective diffusion provide consistent descriptions of the pattern of relaxation. Thus, we may identify the fully ergodic states by the fact that all the elements of the (self- and collective) propagators decay to zero, whereas the fully nonergodic states can be identified by the decay of *all* the propagators to finite asymptotic values

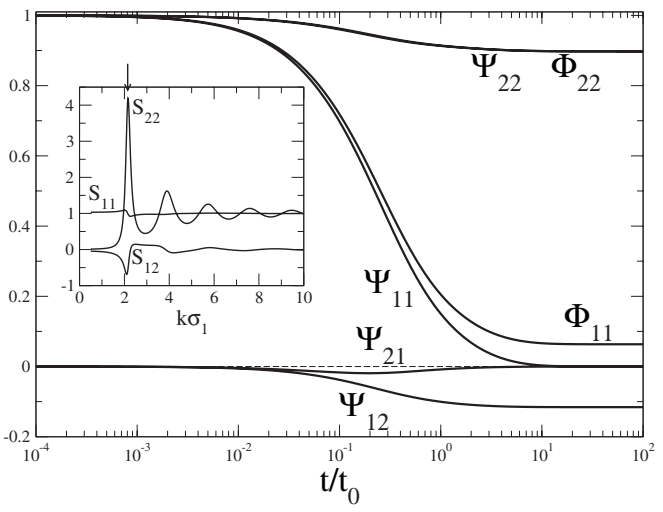

FIG. 4. Collective diffusion propagators $\Psi_{\alpha\beta}(k,t)$ and diagonal collective diffusion correlators $\Phi_{\alpha\alpha}(k,t)$ at a common wave vector corresponding to the position of the main peak of $S_{22}(k)$ (see the inset, which contains static structure factors at this state) for the hard-sphere mixture with $\delta=0.3$ and $x_1=0.2$ for the hybrid state with $\phi=0.55$.

(identified with the nonergodic parameters ψ and $\psi^{(s)}$). The results for $\phi=0.53$ in Fig. 3 are representative of fully ergodic states, whereas those for $\phi=0.57$ illustrate fully arrested states. Hybrid states are characterized by a mixed behavior, in which the diagonal propagators $\Psi_{11}(k,t)$ and $\Psi^{(s)}_{11}(k,t)$ associated with the mobile species decay to zero, while the diagonal propagators $\Psi_{22}(k,t)$ and $\Psi^{(s)}_{22}(k,t)$, associated with the large particles, exhibit arrested behavior. These conditions are illustrated in Fig. 3 by the results corresponding to $\phi=0.55$.

The relaxation of the crossed collective propagators $\Psi_{12}(k,t)$ and $\Psi_{21}(k,t)$, not shown in Fig. 3, do deserve some discussion, particularly in connection with mixed states. First, one must have in mind that, although the matrices $F(k,t)$ and $S(k)$ are symmetric, their product $F(k,t)S^{-1}(k)=\Psi(k,t)$ in general is not; thus, in general, $\Psi_{12}(k,t)\neq\Psi_{21}(k,t)$. Second, since the initial value $\Psi(k,0)$ of the propagator matrix is the unit matrix, the initial value of the off-diagonal collective propagators $\Psi_{12}(k,t)$ and $\Psi_{21}(k,t)$ must vanish. Third, the off-diagonal collective propagators are not necessarily positive. This is illustrated in Fig. 4, which exhibits the time relaxation of the four collective propagators $\Psi_{\alpha\beta}(k,t)$ for the same mixed state included in Fig. 3, but now evaluated at a common wave vector k. The wave vector employed in this figure corresponds to the position of the maximum of $S_{22}(k)$; for reference, the inset of this figure contains the partial static structure factors of this system. At this wave vector we observe that both $\Psi_{12}(k,t)$ and $\Psi_{21}(k,t)$ are negative and that $\Psi_{12}(k,t)$ relaxes to a finite nonergodic asymptotic value, while $\Psi_{21}(k,t)$ is always much smaller and relaxes to zero.

Let us mention that one could also display the same information not in terms of *propagators*, but in terms of the so-called collective "correlators" $\Phi_{\alpha\beta}(k,t)$, defined as $\Phi_{\alpha\beta}(k,t)\equiv F_{\alpha\beta}(k,t)/S_{\alpha\beta}(k)$. Thus defined, the diagonal col-

lective correlator $\Phi_{\alpha\alpha}(k,t)$ is a linear combination of the corresponding diagonal collective propagator $\Psi_{\alpha\alpha}(k,t)$ and of a crossed propagator; more precisely, $\Phi_{11}(k,t)=\Psi_{11}(k,t)+[S_{21}(k)/S_{11}(k)]\Psi_{12}(k,t)$ and $\Phi_{22}(k,t)=\Psi_{22}(k,t)+[S_{12}(k)/S_{22}(k)]\Psi_{21}(k,t)$. In the latter case, since $\Psi_{21}(k,t)$ is small and relaxes to zero, we find that the collective correlator $\Phi_{22}(k,t)$ is virtually identical to the collective propagator $\Psi_{22}(k,t)$, as shown in Fig. 4. In contrast, although the propagator $\Psi_{11}(k,t)$ does decay to zero, the diagonal collective correlator $\Phi_{11}(k,t)$ exhibits dynamic arrest due to its linear dependence on $\Psi_{12}(k,t)$ which, as illustrated in the figure, relaxes to a nonzero value. This observation may be relevant when describing the hybrid states above. For example, the description in terms of correlators has been employed in recent work [30,36,42], where the situation illustrated in Fig. 4 arises, leading to the notion that collective diffusion in mixtures is intrinsically different from self-diffusion. Our results indicate, however, that this apparent difference is just the result of the normalization convention employed in the definition of the correlators and that if the same information were displayed in terms of the elements of the propagator matrices, no mixing of relaxation modes would occur that suggest this notion. We should stress that the *self*-correlators, defined as $\Phi^{(s)}_{\alpha\beta}(k,t)\equiv F^{(s)}_{\alpha\beta}(k,t)$, are identical to the self-propagators $\Phi^{(s)}_{\alpha\beta}(k,t)$ and hence correctly describe the fact that only the small particles diffuse and the large particles are arrested.

Finally, let us mention that distinguishing the three dynamic states above (fully ergodic, fully nonergodic, and hybrid states) with only the information of the type in Figs. 3 and 4 is not a simple matter. The reason is that the nonergodic parameters of the propagators associated with the localization of the small spheres do not jump discontinuously from zero to a finite appreciable value at $\phi_g^{(2)}$. Instead, they increase continuously from a value of zero right at this transition and, hence, attain finite but very small values in the close neighborhood of the transition. In the following section, however, we shall derive a simpler procedure to precisely locate these transitions and to evaluate the nonergodic parameters in the (partially or totally) arrested states.

V. LONG-TIME STATIONARY SOLUTIONS

With the information just presented, one may choose to analyze the detailed time dependence of the propagators and discuss the various regimes of the relaxation processes described by these functions at specific points in the state space. Alternatively, one can discuss more global properties, such as the general topology of the ergodic-nonergodic phase diagram of the system, just like one does in equilibrium statistical thermodynamics. In fact, the ergodic-nonergodic phase diagram should be an important complement to conventional equilibrium phase diagrams in terms of practical applications. If one is interested specifically in such global properties, in principle one does not need to solve the set of coupled equations (2.1)–(2.6) for the full time and wave-vector dependence of all the dynamic properties involved. Instead, one may solve only the so-called bifurcation equations—i.e., the equations for the long-time asymptotic stationary solutions of the full SCGLE theory. The solutions thus determined are precisely the nonergodicity parameters, whose zero or nonzero value reveals if the state of the system is ergodic or dynamically arrested.

In order to derive the fixed-point equations, let us define the nonergodicity parameters of the dynamic properties $\Psi(t)$, $\Psi^{(s)}(t)$, $C(t)$, $C^{(s)}(t)$, and $\Delta\zeta^*(t)$ as the matrices $\psi(k)\equiv\lim_{t\to\infty}\Psi(k,t)$, $\psi^{(s)}(k)\equiv\lim_{t\to\infty}\Psi^{(s)}(k,t)$, $c(k)\equiv\lim_{t\to\infty}C(k,t)$, $c^{(s)}(k)\equiv\lim_{t\to\infty}C^{(s)}(k,t)$, and $\Delta\zeta^{*(\infty)}\equiv\lim_{t\to\infty}\Delta\zeta^*(t)$, respectively. All the elements of these matrices are zero in a fully ergodic state, and the nonzero value of some or all of them indicates partial or total nonergodicity. Let us now substitute the dynamic properties involved in the self-consistent system of equations in Eqs. (2.1)–(2.6) by the sum of their asymptotic long-time value above plus the rest (which, by definition, always relaxes to zero). In the resulting system of equations, let us then take the asymptotic long-time limit, thus generating the following self-consistent system of equations for the nonergodicity parameters:

$$\psi(k)=[c(k)+k^2DS^{-1}(k)]^{-1}c(k), \tag{5.1}$$

$$\psi^{(s)}(k)=[c^{(s)}(k)+k^2D]^{-1}c^{(s)}(k), \tag{5.2}$$

$$c(k)=c^{(s)}(k), \tag{5.3}$$

$$c^{(s)}(k)=\lambda(k)\Delta\zeta^{*(\infty)}, \tag{5.4}$$

and

$$\Delta\zeta_\alpha^{*(\infty)}=\frac{D_\alpha^0}{3(2\pi)^3}\int d^3k\, k^2[\psi^{(s)}]_{\alpha\alpha}[c\sqrt{n}\psi\sqrt{n}h]_{\alpha\alpha}, \tag{5.5}$$

where the matrices c and h inside the integral in the last equation refer to the direct and total Ornstein-Zernike correlation functions and, together with the matrix $\sqrt{n}$, were defined below Eq. (2.6). Using Eqs. (5.3) and (5.4) in Eqs. (5.1) and (5.2), we can express the nonergodicity parameters $\psi(k)$ and $\psi^{(s)}(k)$ in terms of $\Delta\zeta^{*(\infty)}$. Substituting the resulting expressions in Eq. (5.5), we finally get the following closed equation for $\Delta\zeta^{*(\infty)}$:

$$\Delta\zeta_\alpha^{*(\infty)}=\frac{D_\alpha^0}{3(2\pi)^3}\int d^3k\, k^2\{[\lambda(k)+k^2(\Delta\zeta^{*(\infty)})^{-1}D]^{-1}\lambda(k)\}_{\alpha\alpha}(c\sqrt{n}\{[\lambda(k)+k^2(\Delta\zeta^{*(\infty)})^{-1}DS^{-1}(k)]^{-1}\lambda(k)\}\sqrt{n}h)_{\alpha\alpha}, \tag{5.6}$$

for $\alpha=1,2,\ldots,\nu$, with ν being the number of species. Clearly, this equation always admits the trivial solutions $\Delta\zeta_\alpha^{*(\infty)}=0$, which corresponds to the fully ergodic fluid state. The existence of other nonzero real solution(s) is associated with the existence of arrested states.

It is convenient to rewrite Eq. (5.6) in terms of the diagonal matrix $\gamma\equiv(\Delta\zeta^{*(\infty)})^{-1}D$, whose diagonal elements γ_α will then satisfy the set of equations

$$\frac{1}{\gamma_\alpha} = \frac{1}{3(2\pi)^3}\int d^3k\, k^2 \{[I + k^2\gamma\lambda^{-1}(k)]^{-1}\}_{\alpha\alpha}\{c\sqrt{n}[I + k^2\gamma\lambda^{-1}(k)S^{-1}(k)]^{-1}\sqrt{n}h\}_{\alpha\alpha}. \quad (5.7)$$

For the same reasons given in the monocomponent case [17,18], the new order parameters γ_α may be identified with the long-time asymptotic value of the mean-squared displacement (MSD) of particles of species α. Thus, γ_α is infinite if that species diffuses and is finite if it is arrested; in fact, in the latter case $\gamma_\alpha^{1/2}$ is the localization length of the particles of that arrested species. In terms of γ, Eqs. (5.1) and (5.2) for the nonergodicity parameters $\psi(k)$ and $\psi^{(s)}(k)$ read

$$\psi(k) = [I + k^2\gamma\lambda^{-1}(k)S^{-1}(k)]^{-1} \quad (5.8)$$

and

$$\psi^{(s)}(k) = [I + k^2\gamma\lambda^{-1}(k)]^{-1}. \quad (5.9)$$

Equations (5.7)–(5.9) are the fixed-point equations of the SCGLE theory. In the particular case of a monodisperse system, one recovers the result derived and employed in Refs. [17,18]. For a given system—i.e., for given pair potentials—one is supposed to determine first the static structure factor $S_{\alpha\beta}(k)$, which is the only external input in Eq. (5.7) [recall that the matrix $\lambda(k)$ is determined by these structural properties according to Eq. (2.4)]. Equations (5.7) can be solved numerically, and the solutions for γ are then employed in Eqs. (5.8) and (5.9) to determine the nonergodicity parameters.

Let us apply Eqs. (5.7) to calculate the order parameters γ_1 and γ_2 for binary hard-sphere mixtures. The corresponding partial static structure factors $S_{\alpha\beta}(k)$ needed in that equation will again be provided by the Percus-Yevick (PY) approximation. From the resulting values of γ_1 and γ_2, we can classify the states of this system as ergodic, fully nonergodic, or partially nonergodic and thus scan the state space to determine the regions of these dynamic phases and the boundaries between them. For this, let us adopt the asymmetry parameter δ, the total volume fraction ϕ, and the molar fraction x_1 of the smaller spheres as the dimensionless state variables spanning the state space (δ, ϕ, x_1).

Before presenting the results of this exercise, which we collect in Fig. 5, let us say that from intuitive arguments one may advance some of the features of this phase diagram. For example, as already indicated in Sec. IV one expects that for mild asymmetries the only possible mode of dynamic arrest for all volume fractions and all molar fractions is that in which both species are arrested simultaneously. The reason for this expectation is that this regime must contain the extreme case corresponding to the degenerate limit $\delta=1$. From the point of view of their interactions, in this limit the particles of both species are actually indistinguishable ($\sigma_1 = \sigma_2$), thus being in fact a monodisperse system, whose particles have been classified only artificially as belonging to either of these two species. We expect, then, that for any molar fraction $0 \le x_1 \le 1$, the system will be arrested at the total volume fraction $\phi_g^{(m)}$ at which a monodisperse system would be arrested. This means that in the plane $(\delta = 1, \phi, x_1)$, the transition line must correspond to the condition $\phi_1 + \phi_2 = \phi_g = \phi_g^{(m)}$. According to the monocomponent version of the SCGLE theory and within the same level of approximation adopted here for the static structure factor (i.e., the PY approximation) we know that $\phi_g^{(m)} = 0.537$ [18]. Thus, in the degenerate case the straight line $\phi = \phi_g^{(m)}$ [hori-

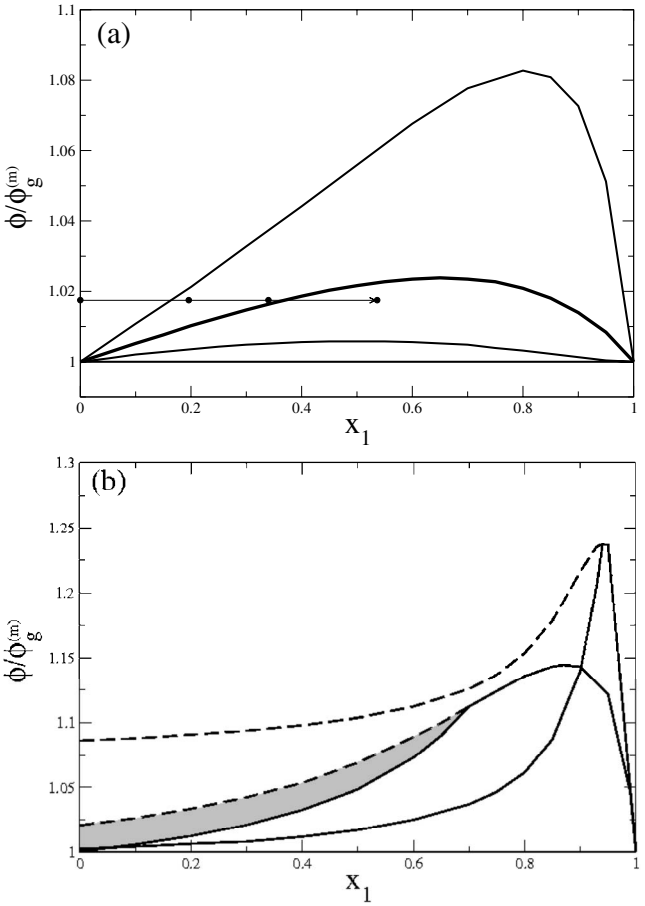

FIG. 5. Phase diagram of dynamic arrest states of the binary hard-sphere mixture. The three-dimensional state space (δ, ϕ, x_1) is spanned by the size disparity parameter $\delta \equiv \sigma_1/\sigma_2 \le 1$, the total volume fraction $\phi \equiv \phi_1 + \phi_2$ with $\phi_\alpha \equiv \pi n_\alpha \sigma_\alpha^3/6$, and the molar fraction of the smaller particles, $x_1 \equiv n_1/(n_1+n_2)$, where σ_α and n_α are the hard-core diameter and the number concentration of particles of species α. This state space is partitioned in three regions corresponding to fully ergodic, mixed, and fully nonergodic states. In this figure we show the intersection lines of this transition surface with the planes of constant δ. The total volume fraction ϕ has been scaled with the volume fraction $\phi_g^{(m)}$ of the ideal glass transition of the monodisperse hard-sphere system. In (a) we illustrate the regime of moderate-size disparities with the values $\delta=1.0$ (horizontal line, corresponding to $\phi=\phi_g^{(m)}$), 0.8, 0.6 (thicker line), and 0.4, where the respective line divides the subspace (ϕ, x_1) in the regions of fully ergodic states (below the line) and fully nonergodic states. The four dots linked by the arrow at fixed total volume fraction $\phi/\phi_g^{(m)} = 1.0175$ correspond to the states prepared in the experiment of Williams and van Megen [29] for $\delta=0.6$. In (b) we illustrate the regime of severe size disparities with the values $\delta=0.3$ and 0.2. In this regime the region of fully ergodic states also lies below the solid line but a region of mixed states appear (shaded region for the case $\delta=0.3$). This region is bounded from above by the localization transition of the small particles (dashed lines).

zontal line in Fig. 5(a)] separates the ergodic region $\phi < \phi_g^{(m)}$ from the region $\phi > \phi_g^{(m)}$ of totally nonergodic states, in which both species are dynamically arrested.

Thus, the first question is now if the SCGLE theory has built in this degenerate limit—i.e., if, under these degenerate conditions, Eqs. (5.7)–(5.9) reduce to the monodisperse result discussed in Refs. [17,18]. Indeed, if one constrains the solution for γ_1 and γ_2 to exhibit this symmetry—i.e., that $\gamma_1 = \gamma_2$—one can show that the two equations involved in Eq. (5.7) are indeed identical to each other and to the corresponding monodisperse equation, independently of the composition represented by the molar fraction x_1. This means that both "species" either remain ergodic or are arrested together.

The next question is then what happens when this degeneracy is broken, so that $\sigma_1 \leq \sigma_2$, but remaining in the region of mild asymmetry $\delta \lesssim 1$, in which we expect small deviations from the degenerate limit. Unfortunately, we do not have good intuitive arguments to anticipate even the sign of these deviations. In Fig. 5(a), however, we report the predictions of our theory for this regime in terms of the glass transition lines corresponding to the values of the asymmetry parameter $\delta=1.0$, 0.8, 0.6, and 0.4, for which our theory predicts that the glass transition line moves to higher total volume fractions ϕ_g as the size disparity increases (i.e., δ decreases), except at the two ends $x_1=0$ and $x_1=1$ of the transition line, where the value of ϕ_g must be fixed by its monodisperse value $\phi_g^{(m)}$ for all size disparities.

The general trends illustrated by Fig. 5(a) were actually first observed and described by Williams and van Megen [29] in their experimental process of melting an originally monodisperse glass by the replacement of a fraction of its particles by particles of a smaller size, keeping the same total volume fraction. The dots and arrow in Fig. 5(a) correspond to their experimental process, which may conceptually be described as driving a system from the initially monodisperse glass state $(\delta, \phi/\phi_g^{(m)}, x_1)=(0.6, 1.0175, 0.0)$ through the arrested states (0.6,1.0175,0.196) and (0.6,1.0175,0.340) to end in the ergodic state (0.6,1.0175,0.537) which lies in the ergodic region according to our predictions for the same size asymmetry $\delta=0.6$ of the experimental system [the representation of this process in the scale of Fig. 5(a) involves the rescaling of the experimental volume fractions $\phi^{exp}=0.58$ with the experimental value of $\phi_g^{(m)}$, which, within the experimental errors, we took as $\phi_g^{(m)}=0.57$].

The regime illustrated in Fig. 5(a) was also studied by Götze and Voigtmann with MCT [37,38] with predictions qualitatively similar to ours for intermediate-size-disparities ($\delta \lesssim 0.65$), but with conflicting predictions for milder size disparities ($\delta \sim 0.8$), where MCT predicts "S-shaped" transition lines that may go below the monodisperse glass transition volume fraction $\phi_g^{(m)}$ [37]. The SCGLE theory predicts, instead, that the transition lines for the mixture, as illustrated in Fig. 5(a) always lie above the horizontal transition line corresponding to the degenerate monodisperse case. These conflicting predictions of MCT and the SCGLE theory could be resolved by experiments and/or computer simulations. The actual magnitude of the difference between the predictions of the two theories is, however, so small that a conclusive discrimination between them will require experimental or simulation results of higher resolution than provided by the currently available data [7,39].

Figure 5(b) illustrates the regime of large-size disparities. The SCGLE theory predicts that below a threshold asymmetry $\delta_c \sim 0.4$, a region of mixed states appears, which is illustrated by the shaded area in the results for $\delta=0.3$. This region is bounded on the left by the axis $x_1=0$, below by the transition of dynamic arrest of the large particles (solid line), and above by the localization transition of the small particles (dashed line). The region of mixed states ends on the right in the bifurcation point where these two transition lines meet and where the transition of simultaneous dynamic arrest of both species starts, ending in the axis $x_1=1$ (solid line). The area of the shaded region increases as δ decreases, as illustrated by the results for $\delta=0.2$, in which the region of mixed states was not shaded. Of course, as δ approaches the threshold value $\delta_c \sim 0.4$, the bifurcation point moves to the axis $x_1=0$ and the region of mixed states disappears. Although we cannot in practice explore the limit $\delta \ll 1$, we do not expect additional qualitatively different trends beside those exhibited by the illustrative cases in Fig. 5. Thus, this figure outlines the entire ergodic-nonergodic phase diagram of a binary hard-sphere mixture.

VI. NONERGODICITY PARAMETERS

The squared localization lengths γ_α are perhaps the simplest order parameters to describe the dynamic arrest transitions in a colloidal mixture. The physics of the transition, however, is described in more detail by the wave-vector dependence of the nonergodicity parameters associated with the normalized intermediate-scattering functions. These may be defined as in the previous section—namely, in terms of the propagator matrices—as $\psi(k) \equiv \lim_{t\to\infty} \Psi(k,t)$ and $\psi^{(s)}(k) \equiv \lim_{t\to\infty} \Psi^{(s)}(k,t)$. One can also define them in terms of the correlator matrices as $f(k) \equiv \lim_{t\to\infty} \Phi(k,t)$ and $f^{(s)}(k) \equiv \lim_{t\to\infty} \Phi^{(s)}(k,t)$. In this section we illustrate some of the main features observed in these parameters.

Figure 6 illustrates the evolution of the wave-vector dependence of the nonergodicity parameters $f_{\alpha\alpha}(k)$ associated with the collective correlators $\Phi_{\alpha\alpha}(k,t)=F_{\alpha\alpha}(k,t)/S_{\alpha\alpha}(k)$ for the case of a moderately size asymmetric hard-sphere mixture ($\delta=0.8$). As discussed before, in this regime the only mode of dynamic arrest is the transition in which both species are simultaneously arrested. Figure 6 illustrates the evolution of the nonergodicity parameters along this glass transition line, as we vary the composition from one extreme condition in which there is only a trace of trapped small particles in a monocomponent hard-sphere glass of larger particles ($x_1=0$, solid lines) to the other extreme condition in which there are a few isolated large particles in a monocomponent hard-sphere glass of smaller particles ($x_1=1.0$, dashed lines). The dotted lines correspond to a representative intermediate condition $x_1=0.4$.

Let us notice that $f_{11}(k)$ becomes increasingly more structured as the molar fraction x_1 is increased from the extreme condition $x_1=0$, in which it decays with k in a smooth bell-shaped manner (solid curve) to the other extreme ($x_1=1.0$, dashed line) where one recognizes the typical wave-vector

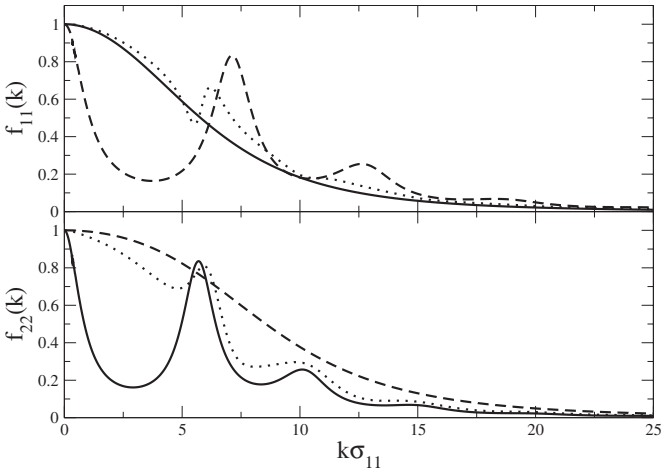

FIG. 6. Nonergodicity parameters $f_{\alpha\alpha}(k)$ associated with the collective correlators $\Phi_{\alpha\alpha}(k,t)$ of a hard-sphere mixture with size-asymmetry $\delta=0.8$ at three states along the glass transition curve corresponding to molar fractions $x_1=0$ (solid line), $x_1=0.4$ (dotted line), and $x_1=1.0$ (dashed line).

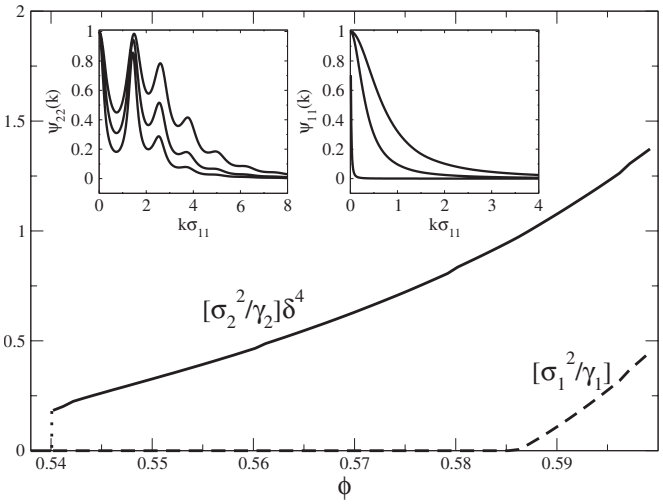

FIG. 7. Evolution of the squared localization length γ_1 and γ_2 of a hard-sphere mixture of size asymmetry $\delta=0.2$ when we increase the total volume fraction ϕ at fixed molar fraction $x_1=0.2$. The solid curve represents $[\sigma_2^2/\gamma_2]\delta^4$, and the dashed curve represents $[\sigma_1^2/\gamma_1]$. The insets display the evolution of the nonergodicity parameters $\psi_{\alpha\alpha}(k)$ as the total volume fraction is increased at fixed $x_1=0.2$. The results for $\psi_{22}(k)$, from bottom to top, correspond to $\phi=0.5402$ $(=\phi_g^{(1)})$, 0.56, and 0.60, and the results for $\psi_{11}(k)$ correspond to $\phi=0.586$ $(=\phi_g^{(2)})$, 0.59, and 0.60.

dependence of the nonergodicity parameter of a monodisperse hard-sphere glass. Essentially the same evolution is observed in $f_{22}(k)$, but in the opposite order, with $f_{22}(k)$ representing, in the limit $x_1=1$, the localization of isolated large particles in a monodisperse glass of smaller particles. A simple description of these two limiting conditions is provided by Eq. (5.8) in the corresponding limit (in which, incidentally, the difference between propagators and correlators vanish). For example, in the limit $x_1\to 1$, one recovers the result for the nonergodicity parameter of a monodisperse system [18], $f_{11}(k)=\psi_{11}(k)=[1+k^2\gamma_1/S_{11}(k)\lambda_{11}(k)]^{-1}$, whereas in the opposite limit $(x_1\to 0)$ one obtains $f_{11}(k)=\psi_{11}(k)=[1+k^2\gamma_1/\lambda_{11}(k)]^{-1}$. The latter is the expression for the nonergodicity parameter of the *self*-diffusion propagator of a monodisperse system, except that in the present case the function $\lambda_{11}(k)\equiv 1/[1+(k/k_{\min}^{(1)})^2]$ involves the wave vector $k_{\min}^{(1)}$ of the location of the first minimum of the partial static structure factor $S_{11}(k)$ of a minority of particles of species 1 in the monodisperse system formed by particles of species 2. Notice the simple but highly non-Gaussian form of this result, which corresponds to the bell-shaped solid curve for $f_{11}(k)$ in Fig. 6. The intermediate conditions represented in this figure by the molar fraction $x_1=0.4$ exhibits the buildup of the structure in going from one of these extreme conditions to the other.

We must mention that the trends just described were first observed and analyzed by Götze and Voigtmann [37] in their MCT results for binary hard-sphere mixtures in the regime of moderate-size asymmetries. There are, of course, rather unimportant quantitative differences, but also relevant qualitative differences to highlight between our present results and those of mode-coupling theory. The most salient of the latter refers to the fact that the small-k limit of the MCT nonergodicity parameter $f_{\alpha\alpha}(k)$ is always smaller than unity, $\lim_{k\to 0} f_{\alpha\alpha}^{(MCT)}(k)<1$, while in the SCGLE theory this limit is always unity, as clearly seen in the results of Fig. 6. This difference vanishes at low concentrations of species α, $x_\alpha\approx 0$, but is quite notorious in the opposite regime $x_\alpha\approx 1$ corresponding to a monodisperse system of species α. The meaning and relevance of these qualitative difference between MCT and the present theory have already been discussed in some detail in the framework of monodisperse systems [18].

The regime of large size disparities offers other interesting issues to discuss. This regime is illustrated in Fig. 7 with the results of the SCGLE theory for a hard-sphere mixture with size-asymmetry $\delta=0.2$. In addition to the simultaneous arrest of the two species, this system may also exhibit partial arrest, in which the large particles become dynamically arrested while the smaller particles continue to diffuse. From Fig. 5 we can see that this transition can be reached by increasing the total volume fraction ϕ of the mixture while keeping the composition fixed at, for example, $x_1=0.2$. Figure 7 describes some aspects of this process. Thus, increasing ϕ at fixed $\delta=0.2$ and $x_1=0.2$ leads to the dynamic arrest of only the large particles at a volume fraction $\phi=\phi_g^{(1)}=0.5402$. Below this volume fraction both species are mobile and their localization lengths are infinite. The main figure illustrates the evolution of γ_2^{-1}, which jumps discontinuously from zero to a finite value as the system passes through this transition (solid line). The nonergodicity parameter $\psi_{22}(k)$ also jumps discontinuously from zero to the value illustrated by the lowest curve in the left inset of the figure. This inset also presents $\psi_{22}(k)$ at two additional volume fractions, one of them $(\phi=0.56)$ within the region of mixed states $\phi_g^{(1)}\le\phi\le\phi_g^{(2)}$ and the other at a volume fraction $(\phi=0.60)$ in the region where both species are dynamically arrested. We observe that in this process the nonergodicity parameter $\psi_{22}(k)$ increases monotonically with ϕ, without exhibiting any special feature as the system crosses the localization transition of the small particles, which occurs at $\phi=\phi_g^{(2)}=0.586$.

Let us now turn to the nonergodicity parameters associated with the small particles. Now we notice that the localization length of these particles remains infinite through the region $\phi_g^{(1)} \leq \phi \leq \phi_g^{(2)}$. This is illustrated by the dashed curve of Fig. 7, which exhibits the evolution of γ_1^{-1} as it crosses the localization transition of the small particles. In contrast with γ_2^{-1}, we now see that γ_1^{-1} does not jump discontinuously from zero to a finite value as the system crosses this transition at $\phi = \phi_g^{(2)} = 0.586$; instead, it departs from zero in a continuous manner. The corresponding behavior of the nonergodicity parameter $\psi_{22}(k)$ is illustrated by the results for this property in the right inset of the figure. Let us finally mention that in Fig. 7 we have employed the nonergodicity parameters $\psi_{\alpha\alpha}(k)$, rather than $f_{\alpha\alpha}(k)$. The main reason for this is that the latter will lead to the rather confusing situation that the nonergodicity parameteter $f_{11}(k)$ will not vanish in the region of mixed states, for the reasons discussed in Sec. III.

VII. CONCLUDING REMARKS

In this paper we have introduced the self-consistent generalized Langevin equation theory of dynamic arrest in colloidal mixtures and we have applied it to the description of dynamic arrest phenomena in two simple model systems—namely, repulsive Yukawa and hard-sphere mixtures—for which we illustrated the scenarios predicted by this theory through the full numerical solution of the coupled system of dynamic equations for the propagators $\Psi(t)$ and $\Psi^{(s)}(t)$ of the self- and collective intermediate scattering functions. In this manner we identified and illustrated the two possible patterns of dynamic arrest in a binary colloidal mixture: namely, the simultaneous and the sequential arrest of the two species. The former corresponds to the transition from the region of fully ergodic states, characterized by infinite values of the order parameters γ_1 and γ_2, to the region of fully nonergodic states, characterized by finite values of these two parameters. This transition is characterized by a discontinuous jump of both order parameters. This is the only dynamic arrest transition possible for moderate-size asymmetry in a binary hard-sphere mixture, as illustrated in Fig. 2. It is also the only transition possible for large asymmetries in the case of hard spheres provided the system is in the limit of a few large particles dispersed in a sea of small particles (the dynamic arrest in the "chancaquilla" limit).

The second pattern of dynamic arrest is only observed for large enough size disparities starting in the regime in which the small particles are a minority. As illustrated in Fig. 3, here the system may be driven from the region of fully ergodic states ($\gamma_1 = \gamma_2 = \infty$) to the region of mixed states (finite γ_2 and $\gamma_1 = \infty$) in which the large particles are arrested and the small ones diffuse through the voids left by the large species. In this transition γ_2 jumps discontinuously from its infinite value in the fully nonergodic region to a finite value in the region of mixed states, whereas γ_1 retains its infinite value. Finally, there is a transition from this region of mixed states to the region of fully ergodic states in which also the small particles are localized (finite values of both γ_1 and γ_2). This latter transition is characterized by a continuous change in the values of both order parameters γ_1 and γ_2, although the latter changes continuously from its infinite value inside the region of mixed states and right at the transition to finite values inside the fully nonergodic region.

Locating the transitions just described may be done by numerically solving the full self-consistent system of equation, as done in Figs. 2 and 3, or by directly determining the nonergodicity parameters, which play the role of order parameters of the transition. The latter can be done more economically through the solution of the "fixed-point" equations. In Sec. IV we derived a strikingly simple and general result for the nonergodicity parameters γ_1 and γ_2, whose use was illustrated with the construction of the phase diagram of the hard-sphere binary mixture. We must say that some of the features of the SCGLE results thus determined were in fact discovered and discussed in the pioneering work of Refs. [32,34–36] based on the multicomponent version of MCT. Our aim here has been to document what is the scenario offered by the SCGLE theory for the same conditions previously studied and to extend the description to aspects not yet discussed with MCT or with other theoretical approaches. In this regard, the main contribution of the present work is the proposal of a theoretical approach that allows the determination of the entire dynamic phase diagram of simple model colloidal mixtures. Thus, the second important contribution involves the simplest of such models: namely, the hard-sphere binary mixture, for which we outlined the entire dynamic arrest phase diagram. In this context we discussed the regime of moderate-size asymmetries, in which we reported the first apparent difference with the results of MCT: namely, the fact that the SCGLE theory does not predict the S-shaped transitions predicted by Götze and Voigtmann [37] on the basis of MCT. For more severe size disparities we also illustrated the main features of the SCGLE predictions, including the precise location of the region of mixed states and its emergence for size disparities beyond a threshold asymmetry $\delta_c \approx 0.4$. These results do not have yet a MCT counterpart to compare with.

In this paper we also discussed the fact that other properties besides γ_1 and γ_2 could be employed as order parameters to classify the various dynamic phases in a mixture. For example, one can use the diagonal elements of the nonergodicity parameters associated with the self-propagator or collective propagator matrices, which also determine unambiguously the various possible states. Although not central to the main subject of this paper, we also explained that the use as order parameters of collective *correlators*, defined as the partial intermediate scattering functions divided by their initial value, may lead to a confusing description of the hybrid states in which one species is arrested and the other remains ergodic.

In summary, we have presented a theory for dynamic arrest phenomena in colloidal mixtures that offers some advantages over the extension to mixtures of conventional MCT. First, it derives from a simpler conceptual formalism, which might allow possible generalizations and extensions. Second,

the resulting equations are much simpler to solve in practice than the corresponding equations of MCT. In fact, the determination of (ergodic-nonergodic) phase diagrams, such as that discussed in the previous section, is considerably simplified in the present case through the use of the results for the nonergodicity parameters γ_α in Eq. (5.7). Thus, many important issues regarding the dynamics and (ergodic-nonergodic) phase behavior of colloidal mixtures may be discussed with the assistance of the SCGLE theory just presented. The implications of the results presented here in the context of specific physical phenomena, and experimental conditions will, however, be the subject of separate reports.

ACKNOWLEDGMENTS

This work was supported by the Consejo Nacional de Ciencia y Tecnología (CONACYT, México), through Grant No. SEP-2004-C01-47611, and FAI-UASLP. The authors are deeply indebted to Professor J. Bergenholtz, Professor A. Banchio, and Professor G. Nägele for useful discussions.

[1] C. A. Angell, Science **267**, 1924 (1995).
[2] P. G. Debenedetti and F. H. Stillinger, Nature (London) **410**, 259 (2001).
[3] W. Götze, in *Liquids, Freezing and Glass Transition*, edited by J. P. Hansen, D. Levesque, and J. Zinn-Justin (North-Holland, Amsterdam, 1991).
[4] P. N. Pusey, in *Liquids, Freezing and the Glass Transition*, edited by J. P. Hansen, D. Levesque, and J. Zinn-Justin (Elsevier, Amsterdam, 1991).
[5] W. Hess and R. Klein, Adv. Phys. **32**, 173 (1983).
[6] G. Nägele, Phys. Rep. **272**, 215 (1996).
[7] W. van Megen and P. N. Pusey, Phys. Rev. A **43**, 5429 (1991).
[8] E. Bartsch *et al.*, J. Chem. Phys. **106**, 3743 (1997).
[9] C. Beck, W. Härtl, and R. Hempelmann, J. Chem. Phys. **111**, 8209 (1999).
[10] K. N. Pham *et al.*, Science **296**, 104 (2002).
[11] F. Sciortino and P. Tartaglia, Adv. Phys. **54**, 471 (2005).
[12] W. Götze and L. Sjögren, Rep. Prog. Phys. **55**, 241 (1992).
[13] G. Szamel, Phys. Rev. Lett. **90**, 228301 (2003).
[14] J. Wu and J. Cao, Phys. Rev. Lett. **95**, 078301 (2005).
[15] P. Mayer, K. Miyazaki, and D. R. Reichman, Phys. Rev. Lett. **97**, 095702 (2006).
[16] M. Tokuyama, Phys. Rev. E **62**, R5915 (2000).
[17] P. Ramírez-González, R. Juárez-Maldonado, L. Yeomans-Reyna, M. A. Chávez-Rojo, M. Chávez-Páez, A. Vizcarra-Rendón, and M. Medina-Noyola, Rev. Mex. Fis. **53**, 327 (2007).
[18] L. Yeomans-Reyna, M. A. Chávez-Rojo, P. E. Ramírez-González, R. Juárez-Maldonado, M. Chávez-Páez, and M. Medina-Noyola, Phys. Rev. E **76**, 041504 (2007).
[19] R. Juárez-Maldonado, M. A. Chávez-Rojo, P. E. Ramírez-González, L. Yeomans-Reyna, and M. Medina-Noyola, Phys. Rev. E **76**, 062502 (2007).
[20] L. Yeomans-Reyna and M. Medina-Noyola, Phys. Rev. E **62**, 3382 (2000).
[21] L. Yeomans-Reyna, H. Acuña-Campa, and M. Medina-Noyola, Phys. Rev. E **62**, 3395 (2000).
[22] L. Yeomans-Reyna and M. Medina-Noyola, Phys. Rev. E **64**, 066114 (2001).
[23] L. Yeomans-Reyna, H. Acuña-Campa, F. de Jesus Guevara-Rodríguez, and M. Medina-Noyola, Phys. Rev. E **67**, 021108 (2003).
[24] M. A. Chávez-Rojo and M. Medina-Noyola, Physica A **366**, 55 (2006).
[25] M. A. Chávez-Rojo and M. Medina-Noyola, Phys. Rev. E **72**, 031107 (2005); **76**, 039902 (2007).
[26] A. Meller and J. Stavans, Phys. Rev. Lett. **68**, 3646 (1992).
[27] A. Imhof and J. K. G. Dhont, Phys. Rev. Lett. **75**, 1662 (1995).
[28] A. Imhof and J. K. G. Dhont, Phys. Rev. E **52**, 6344 (1995).
[29] S. R. Williams and W. van Megen, Phys. Rev. E **64**, 041502 (2001).
[30] A. J. Moreno and J. Colmenero, J. Chem. Phys. **125**, 164507 (2006).
[31] N. Kikuchi and J. Orbach, Europhys. Lett. **77**, 26001 (2007).
[32] J. Bosse and J. S. Thakur, Phys. Rev. Lett. **59**, 998 (1987).
[33] J. L. Barrat and A. Latz, J. Phys.: Condens. Matter **2**, 4289 (1990).
[34] J. S. Thakur and J. Bosse, Phys. Rev. A **43**, 4378 (1991); **43**, 4388 (1991).
[35] J. Bosse and Y. Kaneko, Phys. Rev. Lett. **74**, 4023 (1995).
[36] G. Nägele, J. Bergenholtz, and J. K. G. Dhont, J. Chem. Phys. **110**, 7037 (1999).
[37] W. Götze and Th. Voigtmann, Phys. Rev. E **67**, 021502 (2003).
[38] Th. Voigtmann, Phys. Rev. E **68**, 051401 (2003).
[39] G. Foffi, W. Götze, F. Sciortino, P. Tartaglia, and Th. Voigtmann, Phys. Rev. E **69**, 011505 (2004); Phys. Rev. Lett. **91**, 085701 (2003).
[40] Th. Voigtmann, A. M. Puertas, and M. Fuchs, Phys. Rev. E **70**, 061506 (2004).
[41] E. Flenner and G. Szamel, Phys. Rev. E **72**, 031508 (2005).
[42] Th. Voigtmann and J. Horbach, Europhys. Lett. **74**, 459 (2006).
[43] E. Zaccarelli, H. Löwen, P. P. F. Wessels, F. Sciortino, P. Tartaglia, and C. N. Likos, Phys. Rev. Lett. **92**, 225703 (2004).
[44] In reality, Nägele, Bergenholtz, and Dhont [36] refer to the matrix product $[C(k,z)D]$ as the matrix of "irreducible memory functions," a concept first introduced by B. Cichocki and W. Hess, Physica A **141**, 475 (1987).
[45] G. H. Vineyard, Phys. Rev. **110**, 999 (1958).
[46] B. Cichocki and K. Hinzen, Ber. Bunsenges. Phys. Chem **94**, 243 (1990).
[47] J. L. Arauz-Lara and M. Medina-Noyola, Physica A **122**, 547 (1983).
[48] M. Medina-Noyola, Faraday Discuss. Chem. Soc. **83**, 21 (1987).
[49] M. Medina-Noyola and J. L. del Río-Correa, Physica A **146**, 483 (1987).
[50] M. Hernandez-Contreras, M. Medina-Noyola, and A. Vizcarra-

Rendon, Physica A **234**, 271 (1996).
[51] M. Fuchs, W. Götze, I. Hofacker, and A. Latz, J. Phys.: Condens. Matter **3**, 5047 (1991).
[52] A. J. Banchio, Ph.D. thesis, University of Konstanz, 1999.
[53] J. P. Hansen and I. R. McDonald, *Theory of Simple Liquids* (Academic, New York, 1976).
[54] Chancaquilla is one of the many names for one of the many versions of this candy, in this case made with pumpkin and sesame seeds in the Rio Verde region of the Mexican state of San Luis Potosí.
[55] J. L. Lebowitz, Phys. Rev. **133**, A895 (1964).